Dynamic response of silicon nanostructures at finite frequency: An orbital-free density functional theory and non-equilibrium Green's function study

Fuming Xu, Bin Wang, Yadong Wei, and Jian Wang

Citation: Journal of Applied Physics **114**, 153703 (2013); doi: 10.1063/1.4825127
View online: http://dx.doi.org/10.1063/1.4825127
View Table of Contents: http://scitation.aip.org/content/aip/journal/jap/114/15?ver=pdfcov
Published by the AIP Publishing

JOURNAL OF APPLIED PHYSICS **114**, 153703 (2013)

Dynamic response of silicon nanostructures at finite frequency: An orbital-free density functional theory and non-equilibrium Green's function study

Fuming Xu,[1] Bin Wang,[1,2] Yadong Wei,[2] and Jian Wang[1,a)]
[1]*Department of Physics and the Center of Theoretical and Computational Physics, The University of Hong Kong, Hong Kong, China*
[2]*Department of Physics and Institute of Computational Condense Matter Physics, Shenzhen University, Shenzhen 518060, China*

(Received 22 April 2013; accepted 30 September 2013; published online 16 October 2013)

Orbital-free density functional theory (OFDFT) replaces the wavefunction in the kinetic energy by an explicit energy functional and thereby speeds up significantly the calculation of ground state properties of the solid state systems. So far, the application of OFDFT has been centered on closed systems and less attention is paid on the transport properties in open systems. In this paper, we use OFDFT and combine it with non-equilibrium Green's function to simulate equilibrium electronic transport properties in silicon nanostructures from first principles. In particular, we study ac transport properties of a silicon atomic junction consisting of a silicon atomic chain and two monoatomic leads. We have calculated the dynamic conductance of this atomic junction as a function of ac frequency with one to four silicon atoms in the central scattering region. Although the system is transmissive with dc conductance around 4 to 5 e^2/h, capacitive-like behavior was found in the finite frequency regime. Our analysis shows that, up to 0.1 THz, this behavior can be characterized by a classic RC circuit consisting of two resistors and a capacitor. One resistor gives rise to dc resistance and the other one accounts for the charge relaxation resistance with magnitude around $0.2\,h/e^2$ when the silicon chain contains two atoms. It was found that the capacitance is around 5 aF for the same system. © *2013 AIP Publishing LLC*. [http://dx.doi.org/10.1063/1.4825127]

I. INTRODUCTION

With the rapid development of nanotechnology, electronic transport study in nano-devices has attracted increasingly theoretical and experimental research interests in the past few decades. In modeling the functionality of nanostructures, the *ab initio* methods are widely used for ground state properties of isolated or periodic systems since they are very accurate and parameter free. For open systems, one of the important formalisms to study transport properties from first principles is the Kohn-Sham density functional theory (KSDFT) combined with non-equilibrium Green's function (NEGF) method. KSDFT[1] has been successfully employed in computation of ground state properties of electronic systems.[2] On the other hand, NEGF theory[3] is capable of describing systems which have many body interactions and are far away from equilibrium. The combination of them, KSDFT-NEGF formalism,[4,5] is currently the most popular approach in first principles investigation of non-equilibrium quantum transport of nanostructures. In this formalism, electron density of the non-equilibrium system is constructed from the lesser Green's function as a function of the KS Hamiltonian, which connects the KSDFT and NEGF. The KSDFT-NEGF method has been realized in several simulation software, for instance, MatDcal,[6] NanoDcal,[4,7] ABINIT,[8] and ATK.[5,9] It has been regarded as one of the standard techniques in non-equilibrium transport study of nanoscale devices. However, the heavy numerical cost of KSDFT has limited its application on large-scale systems. Generally speaking, the NEGF combined with KSDFT formalism is appropriate for studying systems with thousands of atoms. Moreover, the self-consistent solution of KSDFT-NEGF could be very difficult to reach for large systems. This is because the charge transfer is the salient feature in quantum transport and it is much harder to re-distribute the charge for large systems. Since a typical nanostructure usually contains dozens of thousands of atoms, it is very difficult to achieve a self-consistent calculation within KSDFT-NEGF methodology and a huge computation resource is required.

On the other hand, together with the progress in constructing more accurate density functionals, orbital-free density functional theory (OFDFT)[10,11] has regained many research interests for large scale calculation. It has been used to numerically simulate equilibrium properties of a metallic system with 1×10^6 aluminum atoms,[12] showing the potential application in large systems. Compared with KSDFT, OFDFT has its advantage on linear-scaling with the number of degrees of freedom and existence of minimization principle. The trade-off is on the numerical accuracy, which mainly arises from the lack of single electron orbital orthonormalization. At present, the difference between OFDFT simulation on some bulk properties and that from the KSDFT has been reduced to several percent for a variety of materials.[13] Very recently, there is a breakthrough of OFDFT simulation on transition metal.[14] Using the electron density decomposition technique, the OFDFT simulation of many bulk properties on Ag can quantitatively reproduce the KSDFT predictions.[14] There are also progress on benchmark test on OFDFT in comparison with KSDFT. In Ref. 15, it was found that the OFDFT-calculated bond dissociation

a)Electronic address: jianwang@hku.hk

energy, equilibrium bond length, and vibrational frequency of a variety of homonuclear diatomic molecules are in remarkably good agreement with that of KSDFT results. OFDFT has also been used to calculate the transport properties in open two dimensional quantum structures, which allows us to examine the effect of exchange and correlation effect on transport, in addition to direct Coulomb interaction.[16,17] In this calculation, the potential landscape has been calculated within Thomas-Fermi-Dirac-von Weizsacker formalism and atomic core has been approximated using jellium model. Given successful application of OFDFT in equilibrium systems, it is important and timely to apply OFDFT method in fully atomic study of transport through nanostructures.

In this paper, we have applied OFDFT in transport calculation of nano-devices when the system is in equilibrium. Different from periodic systems or isolated molecular systems, a transport calculation deals with an open system (see Fig. 1). In the *screening approximation*,[19] the problem is solved in two steps. First, the potential profiles of two semi-infinite leads are computed with periodic boundary conditions, which will be used as the boundary conditions for the central scattering region. Then, the potential landscape is solved for the central scattering region with the boundary conditions calculated from leads. Second, once the potential landscape is known the transport properties are calculated using NEGF theory. Due to the nature of open systems, we have to choose appropriate density functionals, which are suitable for transport calculation. After some analysis, we decide to use Thomas-Fermi-Dirac-von Weizsäker kinetic energy functional in our calculation. The effective potential is obtained by directly minimizing total energy under the constraint of total number of electrons in the system. Then, the real space ground state effective potential is transformed into linear combination of atomic orbital (LCAO) to construct the single-electron Hamiltonian in orbital space. Next, the Green's function is constructed and the transport properties are calculated within NEGF theory. We performed such calculation on a silicon atomic junction shown in Fig. 1, which contains a single-atomic chain and two body-centered cubic leads extending to infinite long. Numerical results suggest that, ac response of the silicon system at small frequency shows capacitive-like behavior and its dynamic conductance at sub-terahertz is well described by a classic RC circuit. The calculation also reveals that, with the increasing of atom number in the atomic chain, the zero-frequency conductance is reduced and the capacitance of the silicon system is enhanced.

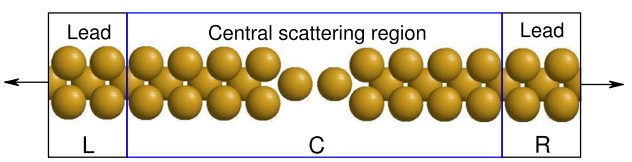

FIG. 1. Schematic representation of a silicon atomic device. The central region contains a silicon chain and two unit cells of the left and right leads, which have simple cubic structure. The two periodic leads extend to infinities, connecting the central region to electron reservoirs. The whole system is under equilibrium condition.

The paper is organized as follows: Sec. II reviews theoretical foundations of OFDFT method, accompanied by the detailed procedure in implementation on open boundary systems. In Sec. III, we use this method to calculate dynamic conductance of a silicon nanostructure and give discussion on the numerical results. Finally, conclusion will be given in Sec. IV.

II. THEORETICAL FORMALISM

In this section, we give a detailed description on applying OFDFT in transport study. Here is our general strategy. First, we divide the system into three regions: central scattering region as well as left and right leads regions. With the proper boundary conditions discussed below, open scattering problem reduces to that in a finite closed system. Second, OFDFT is used to find out the ground-state scattering potential landscape for the closed system. This is a minimization problem and very efficient to converge. Finally, with the converged potential landscape, NEGF is adopted to calculate the transport properties through the atomic junctions. Now we start with the special requirements of applying OFDFT on open boundary systems.

A. OFDFT with open boundaries

It is well known that, in OFDFT, all the energy terms in the total energy expression are explicit functionals of electron density, especially the kinetic energy. The total energy of an electronic system in OFDFT reads

$$E_{tot}^{OF} = T_s[\rho] + E_H[\rho] + E_{xc}[\rho] + \int V_{ps}(\mathbf{r})\rho(\mathbf{r})d\mathbf{r}, \quad (1)$$

where the first term $T_s[\rho]$ is the non-interacting kinetic energy functional of electron density (usually refereed as KEDF, kinetic energy density functional). The second one is the Hartree energy arising from the classical electron-electron interaction. E_{xc} is the exchange-correlation energy functional. The last term is the energy from the pseudopotential of ions. Due to the lack of electron orbitals, the nonlocal pseudopotential[18] in KSDFT has to be replaced by the local pseudopotential (LP). Before presenting these energy density functionals, we should first consider the special requirement in boundary conditions needed for transport calculation.

A typical setup of an atomic device is schematically plotted in Fig. 1. The device consists of a silicon chain, connected by two semi-infinite leads to the electron reservoirs. The transport is through the longitudinal direction and we leave enough vacuum region in the transverse directions and a few atomic layers of leads in the simulation box. To deal with transport properties of this system, we should consider two different kinds of boundary conditions. The two semi-infinite leads can be easily handled with conventional periodic boundary conditions. The central simulation box is an open system, which is neither periodic nor isolated system. To treat the open boundary condition, we adopt the empirical *screening approximation*,[19] which argues that the influence of scattering region is screened by the atomic leads of buffer layer so that the effective potential a few layers away from

the scattering region is close to the effective potential of the lead. A natural boundary condition for the central simulation box is given by[19]

$$V_{eff}(z)|_{central} = V_{eff}(z)|_{lead}, \tag{2}$$

where z labels a surface on the boundary. In principle, Eq. (2) holds for z located deeply enough in the lead. In practice, a few layers of atomic lead can give very good screening. After the self-consistent calculation of OFDFT is done and the ground state of the system is reached, electron density at these surfaces should be equal, which makes sure that the effective potential matches perfectly on the interface. In this way, the open system can be treated as a finite one where variational principle is applicable. Later we will show that, how this treatment affects the choice of energy density functionals when applying OFDFT in open boundary problems. Expressions of each term in Eq. (1) used in our calculation are listed below.

1. Kinetic energy density functional $T_s[\rho]$

The major difference between KSDFT and OFDFT lies in kinetic energy functional. Unlike the KS kinetic energy which is exactly expressed in terms of the non-interacting single electron orbitals, KEDF does not have an explicit relation with electron density but can be approximated to approach the KS kinetic energy as close as possible. Since the kinetic energy accounts for a large part of the total energy, it affects the accuracy of OFDFT simulation in a crucial way. In the past decades, most research efforts in OFDFT field have been focused on designing more accurate KEDFs. One popular strategy is forcing the KEDF to fulfill the linear response behavior of electron gas. KEDF of this type is usually expressed as[20]

$$\begin{aligned} T_s[\rho] &= T_{TF} + T_{vW} + T_K[\rho], \\ T_{TF}[\rho] &= C_{TF}\int \rho^{5/3}(\mathbf{r})d\mathbf{r}, \quad C_{TF} = \frac{3}{10}(3\pi^2)^{2/3}, \\ T_{vW}[\rho] &= \int \sqrt{\rho(\mathbf{r})}\left(-\frac{1}{2}\nabla^2\right)\sqrt{\rho(\mathbf{r})}d\mathbf{r}, \\ T_K[\rho] &= \int\int \rho^{\alpha}(\mathbf{r})K_{\alpha,\beta}(\mathbf{r}-\mathbf{r}')\rho^{\beta}(\mathbf{r}')d\mathbf{r}'d\mathbf{r}, \end{aligned} \tag{3}$$

where T_{TF} is the Thomas-Fermi kinetic energy[21] derived from homogeneous electron gas and T_{vW} is the von Weizsäker (vW) kinetic energy,[22] which is exact for a bosonic system.

The third term in KEDF, $T_K[\rho]$, has to be approximated according to the Lindhard response function[23] and α and β are parameters to be determined. The nonlocal kernal $K_{\alpha,\beta}(\mathbf{r}-\mathbf{r}')$ was originally designed as electron density independent.[20] Later it was generalized to density dependent version. This linear response KEDF greatly improves the performance of OFDFT in modeling bulk properties of main group metals.[24] Most recently, by forcing the KE to satisfy the correct asymptotic behavior, $T_K[\rho]$ has been extended to simulate semiconductors.[13] To our knowledge, the linear response KEDF represents presently the most accurate kinetic functional which greatly improves the performance of OFDFT in many aspects. But the nonlocal kernal $K_{\alpha,\beta}(\mathbf{r}-\mathbf{r}')$ has to be evaluated in momentum space and usually Fast Fourier transformation (FFT) is required. Hence, periodic boundary conditions are necessary in applying this KEDF, which means that it is not applicable in open boundary problems.

In OFDFT research field, there are also other strategies to construct KEDFs from distinct considerations. For instance, in Ref. 25, constraint-based local approximate KEDF is proposed by requiring that the KE generates adequate interatomic forces, not total energies nor general linear response. This type of KEDF is particularly suitable for multiscale molecular-dynamics (MD) simulations. Another kind of KE is constructed as T_{vW}, the exact KE for bosonic systems, plus one or more positive-definite terms arising from the fermi nature of electrons, which also attracts considerable research interest.[26] The generalized-gradient-approximation (GGA) type KEDF also has a long history[27] and new developments are continuously made.[28]

Given these choices of KEDFs, our primary concern is easy to implement in open boundary condition and cheap in numerical cost. Based on this consideration, the Thomas-Fermi plus von Weizsäker model[29,30] is chosen as the kinetic energy functional in our calculation, which reads

$$T_s[\rho] = T_{TF} + \lambda T_{vW}, \tag{4}$$

where λ is an adjustable parameter. To ensure the accuracy when evaluating T_{vW}, for the periodic leads we use the FFT technique and for the central region high-order finite difference method is employed.[31] In the latter case, density distribution of a few adjacent layers in the leads is required, which closely connects the central region and leads on the interface.

2. Hartree energy $E_H[\rho]$

The second functional of the total energy defined in Eq. (1) is the classical Hartree energy

$$E_H[\rho] = \frac{1}{2}\int\int \frac{\rho(\mathbf{r})\rho(\mathbf{r}')}{|\mathbf{r}-\mathbf{r}'|}d\mathbf{r}'d\mathbf{r}. \tag{5}$$

Usually, we calculate the Hartree potential first, which is the functional derivative of E_H on density $\rho(\mathbf{r})$

$$V_H(\mathbf{r}) = \int \frac{\rho(\mathbf{r})}{|\mathbf{r}-\mathbf{r}'|}d\mathbf{r}', \tag{6}$$

which is equivalent to solve the Poisson equation

$$\nabla^2 V_H(\mathbf{r}) = -4\pi\rho(\mathbf{r}). \tag{7}$$

To solve the Poisson equation, we use the FFT technique when handling the periodic leads. For the central scattering region, FFT is adopted in the transverse directions since there is enough vacuum region and finite difference method is applied in the longitudinal direction. Potential and density profiles on the interface between the periodic leads and central region are required in this step.

3. Exchange-correlation energy $E_{xc}[\rho]$

The exchange-correlation energy functional can be made as the same in KSDFT, as long as it is only density dependent. One can either use local density approximation (LDA) or GGA type E_{xc}. We adopt LDA in our calculation, which reads

$$E_{xc}[\rho(\mathbf{r})] = \int \rho(\mathbf{r})\varepsilon_{xc}[\rho(\mathbf{r})]d\mathbf{r}, \tag{8}$$

with the short range exchange-correlation energy density given by[33]

$$\varepsilon_{xc} = -\frac{a_0 + a_1 r_s + a_2 r_s^2 + a_3 r_s^3}{b_1 r_s + b_2 r_s^2 + b_3 r_s^3 + b_4 r_s^4} \tag{9}$$

here $r_s = (3/(4\pi\rho))^{1/3}$, defined as the local Seitz radius. Coefficients for different orders of r_s are respectively

$$\begin{aligned} a_0 &= 0.458165 \quad a_1 = 2.217059, \\ a_2 &= 0.740555 \quad a_3 = 0.019682, \\ b_1 &= 1.000000 \quad b_2 = 4.504130, \\ b_3 &= 1.110667 \quad b_4 = 0.023592. \end{aligned} \tag{10}$$

In principle, other types of LDA E_{xc} functional[34] and GGA form E_{xc}[35] are also applicable in OFDFT.

4. Local pseudopotential

The isotropic local pseudopotential represents another error source in OFDFT compared with KSDFT. Historically, local pseudopotentials are defined either in real space[36] or reciprocal space[37] in parameter-dependent forms. Take the silicon atom as an example. Its local pseudopotential was defined in reciprocal space as a function of k[37]

$$V_{ps}(k) = -\frac{4\pi Z a_1}{k^2}[\cos(a_2 k) + a_3]e^{a_4 k^4}. \tag{11}$$

The relevant parameters are, respectively, $a_1 = 2/(1+a_3)$, $a_2 = 0.79065$, $a_3 = -0.35201$, and $a_4 = -0.01807$. The main part of $V_{ps}(k)$ is $-4\pi Z/k^2$, which is the Fourier transform of Coulomb potential $-Z/r$. The exponential term makes sure that $V_{ps}(k)$ does not fluctuate at large k, hence the corresponding pseudopotential in real space recovers the $-Z/r$ form at certain distance.

This type of local pseudopotentials has analytic definitions either in real space or k space with several adjustable parameters. Their simple expressions are convenient to be implemented in calculation of different atomic structures. But the parameters can only be adjusted to properties of one specific structure; they are less accurate to other environments. The poor transferability of these parameter-dependent LPs is unpleasant in computation.

In the past decade, the optimized effective potential (OEP) method[38] was used to design numerical local pseudopotential.[39,40] Employment of these accurate and transferable local pseudopotential systematically improves the performance of OFDFT calculation on many bulk properties. We plot in Fig. 2 the local pseudopotentials of silicon from different definitions. The Ihm and Cohen type LP has a slow transition behavior to $-Z/r$. OEP resultant LP[40] has the most smooth curvature and the hardest core. Both of them are hard potentials and reserve a local maximum at the atom center $r = 0$, which is the genetic feature of local pseudopotential. This hard core represents the repulsion of core electrons to the valence electron, preventing them to accumulate in the closed inner shell. At certain distance, all LPs recover the Coulomb tail $-Z/r$. In the following calculation, we will test the accuracy of these LPs when employed in transport study.

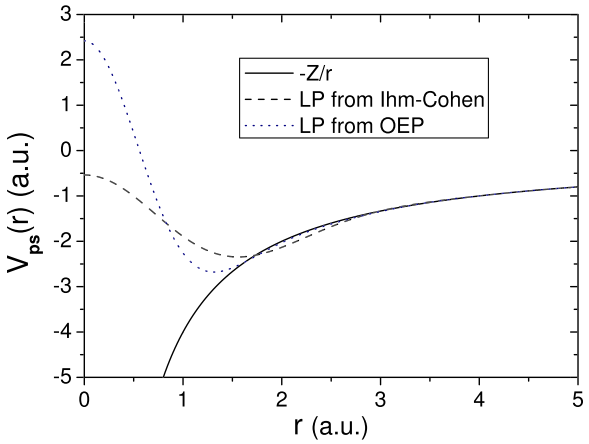

FIG. 2. Local pseudopotentials of silicon defined in reciprocal space, and from optimized effective potential method, respectively. Coulomb potential $-Z/r$ is plotted for comparison.

It is noticed that there are two long-range potentials which have Coulomb tails at large distance L

$$\begin{aligned} V_H(\mathbf{r}) &= \int \frac{\rho(\mathbf{r}')}{|\mathbf{r}-\mathbf{r}'|}d\mathbf{r}' \sim \frac{N_e}{L}, \\ V_{ps}(\mathbf{r}) &\sim -\frac{N_e}{L}. \end{aligned} \tag{12}$$

Ignoring the dipole and higher moments induced by the electron distribution, these two terms cancel to each other at large distance according to the Gauss's law. In periodic systems, V_H and V_{ps} are easily constructed using geometric structure factor and Fourier transform. When periodic boundary condition is absent, the long range behavior results in a heavy numerical burden in real space calculation. Taking advantage of the cancelation of V_H and V_{ps}, their long range influence can be screened by adding and subtracting the potential from a neutral charge density. The neutral charge density around each ion is normalized to $\int \rho_I^{NA}(\mathbf{r})d\mathbf{r} = Z_I$, with Z_I the charge of the *Ith* ion. The screened forms of Hartree potential and pseudopotential are, respectively,[41]

$$\begin{aligned} V_{\delta H} &= \int \frac{(\rho(\mathbf{r}') - \rho^{NA}(\mathbf{r}'))}{|\mathbf{r}-\mathbf{r}'|}d\mathbf{r}', \quad \rho^{NA} = \sum_I \rho_I^{NA}, \\ V_{NA} &= \sum_I V_{NA,I} = \sum_I \left\{ V_{ps,I} + \int \frac{\rho^{NA,I}(\mathbf{r}')}{|\mathbf{r}-\mathbf{r}'|}d\mathbf{r}' \right\}, \end{aligned} \tag{13}$$

where $\int \rho^{NA}(\mathbf{r})d\mathbf{r} = N_e$ makes sure the charge neutrality in the simulation region. This technique is originally from the

SIESTA code and presented in Refs. 9 and 41. Introduction of ρ^{NA} produces short range screened Hartree potential $V_{\delta H}$ and neutral atom potential V_{NA}, and one can easily prove that

$$V_H + V_{ps} = V_{\delta H} + V_{NA} \tag{14}$$

so that the effective potential remains the same. There are two advantages when the neutral atom density is introduced

(1) since V_{NA} is short range, it is numerically convenient and efficient to add up V_{NA} for all the ions.
(2) In practical implementation, it is difficult to match the boundary conditions using Eq. (2). It is more convenient to match the boundary conditions of the screened potential $V_{\delta H}$ induced by charge neutral distribution $\rho(\mathbf{r}) - \rho^{NA}(\mathbf{r})$. The corresponding Poisson equation reads

$$\nabla^2 V_{\delta H}(\mathbf{r}) = -4\pi(\rho(\mathbf{r}) - \rho^{NA}(\mathbf{r})). \tag{15}$$

The detailed technique can be found in Refs. 19 and 32.

Once the total energy functional in Eq. (1) is constructed, the ground state electron density can be reached by minimizing E_{tot}^{OF} with respect to the electron density, which is ensured by the second HK theorem.[1] The theorem also requests two constraints on the electron density

(1) Electron density is non-negative definite, $\rho(\mathbf{r}) \geq 0$.
(2) Number of electrons in the system should be conserved, $\int \rho(\mathbf{r}) d\mathbf{r} = N_e$.

By making a simple variable substitution $\chi = \sqrt{\rho}$ to ensure the first constraint, and defining a new functional

$$\Pi[\rho] = E_{tot}^{OF} - \mu\left(\int \chi^2(\mathbf{r}) d\mathbf{r} - N_e\right) \tag{16}$$

to satisfy the second one. Here, μ is the Lagrangian multiplier, evaluated as the mean value of total energy functional derivative.[10] By variational principle, $\Pi[\rho]$ preserves a minimum value when the system is at its ground state,

$$\frac{\delta \Pi[\rho]}{\delta \rho} = \frac{\delta E_{tot}^{OF}}{\delta \rho} - \mu = 0 \tag{17}$$

or

$$\frac{\delta \Pi}{\delta \chi} = \frac{\delta E_{tot}^{OF}}{\delta \chi} - 2\mu\chi = 0. \tag{18}$$

Equations (17) and (18) provide the numerical condition in reaching the ground state.

Many numerical methods can be used in finding minimum of functional $\Pi[\chi]$. For example, steepest descent method and conjugate gradient methods,[42] truncated Newton method.[10] It is more efficient if the descent direction fulfills the electron number constraint, which can be realized in constructing a normalized direction.[43] When the ground state is reached by direction minimization, we obtain the ground state effective potential of the system, which satisfies the Euler equation

$$\frac{\delta T_s}{\delta \rho} + V_{eff}(\mathbf{r}) = 0. \tag{19}$$

B. Implementation in electronic transport

In OFDFT, we solve the Euler equation to find the ground state effective potential needed for transport calculation. In Matdcal[6] software, the Hamiltonian operator is projected in orbital basis consisted by LCAO.

The atomic orbitals $\{\zeta_\mu\}$ are localized in real space. ζ_μ has the following expression:[19]

$$\zeta_\mu(\mathbf{r} - \mathbf{R_I}) = R_l(|\mathbf{r} - \mathbf{R_I}|)Y_{lm}(\Omega_{\mathbf{r}-\mathbf{R_I}}),$$

where $\mathbf{R_I}$ indicates the position of this atom and R_l is an isotropic radial function, which has a cut-off radius R_{cut}. Here, Y_{lm} is the spherical harmonics function with lm the angular momentum index, containing the other two degrees of freedom in the spherical coordinate system.

In terms of the $\{\zeta_\mu\}$ basis set, the single electron eigenfunction ψ_i in the Kohn-Sham equation is expressed as the linear combination of ζ_μ

$$\psi_i = \sum_\mu c_\mu^i \zeta_\mu.$$

The Kohn-Sham equation is then transformed into

$$H_{\mu\nu} c_\nu^i = \varepsilon_i S_{\mu\nu} c_\nu^i, \tag{20}$$

where $S_{\mu\nu}$ is the overlap matrix describing the overlapping between the orbitals ζ_μ from different atoms. $S_{\mu\nu}$ and the Hamiltonian matrix elements in orbital space read

$$\begin{aligned} S_{\mu\nu} &= \int d\mathbf{r} \zeta_\mu^*(\mathbf{r}) \zeta_\mu(\mathbf{r}), \\ T_{\mu\nu} &= \int d\mathbf{r} \zeta_\mu^*(\mathbf{r}) \left(-\frac{1}{2}\nabla^2\right) \zeta_\nu(\mathbf{r}), \\ V_{eff,\mu\nu} &= \int d\mathbf{r} \zeta_\mu^*(\mathbf{r}) V_{eff} \zeta_\nu(\mathbf{r}). \end{aligned} \tag{21}$$

We can construct Hamiltonian in orbital space once the ground state effective potential is obtained. The advantage of employing the localized orbital basis $\{\zeta_\mu\}$ is that, it leads to a sparse form of the Hamiltonian matrix in orbital space, which greatly reduces the numerical cost in solving the matrix equation. In contrast to the real space grid with a common submillion dimension (a typical $64 \times 64 \times 64$ mesh grid in real space), the single-zeta basis in MatDcal only involves 4 bases (one s orbital and $3p$ orbitals) per electron. Hence, the dimension of orbital space Hamiltonian matrix is rather small. The tradeoff is the loss of accuracy in ζ_μ basis, since it is an incomplete one. Careful attention has to be paid on choosing suitable numbers of ζ_μ bases and their cutoff radii.

In terms of the orbital space Hamiltonian $H_{\mu\nu}$, the retarded Green's function is conventionally defined as[45]

$$G^r = \frac{1}{ES - H - \Sigma^r}, \tag{22}$$

where S is the overlap matrix and Σ^r is the self-energies of the leads, calculated from the lead Hamiltonian in advance. Once G^r is established, transport properties can be computed within the NEGF formalism. At this stage, we have applied OFDFT in electronic transport through open systems. Our code is realized on MatDcal package.[6]

The detailed procedure of applying OFDFT on transport of open systems is schematically plotted in the flowchart of Fig. 3. The LCAO basis set has played a critical role in constructing the single electron Hamiltonian. Compared with the KSDFT-NEGF formalism, the OFDFT method is preferable on these properties:

(1) Linear-scaling numerical cost and fully real space implementation.
(2) No need of frequent transformation between LCAO orbital space and real space needed for solving Poisson equation.
(3) Fast and stable direct minimization algorithm with no charge sloshing.
(4) Low memory cost in the converging process.

These favorable features make the OFDFT method a promising candidate in studying electronic transport of large-scale atomic systems. The validity of variational principle enables fast direct minimization numerical methods, but also limits its applicability on non-equilibrium transport problems. Hence, we can only study systems under equilibrium conditions.

To end this section, we would like to emphasize the key steps to apply OFDFT on equilibrium transport problems. The self-consistent OFDFT simulation on the equilibrium system generates the scattering potential. The Hamiltonian of the system is then constructed on the LCAO basis. With this Hamiltonian, the Green's function is defined in a conventional manner, and the transport properties of the system are investigated within the NEGF theory. In Sec. III, we will discuss the applicability of the OFDFT method on transport study.

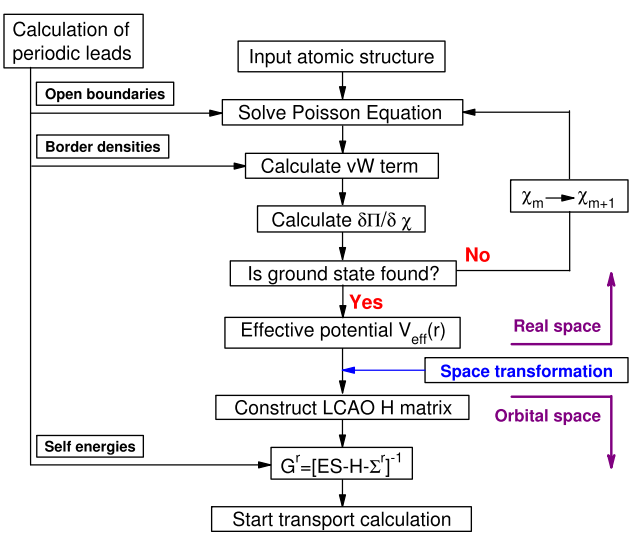

FIG. 3. Flowchart of the OFDFT method on electronic transport, realized on LCAO basis set of the MatDcal package.[6]

III. NUMERICAL RESULTS AND DISCUSSION

In this section, we perform the OFDFT transport study on a silicon atomic structure. The system is depicted in Fig. 1, which has the typical lead-atomic junction-lead setup. The central scattering region of this system contains several silicon atoms and enough buffer layers of the periodic leads. Such kind of single-atomic chain structure has been experimentally realized on Au, Pt, and Ir materials using mechanically controllable break junction technique.[44] It is possible to fabricate a silicon single-atomic chain structure by this technique. The left and right leads are identical and both have body-centered cubic lattices in z direction. Sufficient vacuum has been included in the whole simulation region to make sure that electron density at the x and y boundaries decays to zero. The two leads spread to $\pm\infty$ and connect the electron reservoirs. The whole structure is in equilibrium where the variational principle is applicable. We choose $\lambda = 0.2$ in the T_{vW} kinetic energy functional and 6th order finite difference method[31] with boundary values of electron density interpolated from the leads are used to calculate T_{vW} of the central region. Local pseudopotential is constructed from both analytic method[37] and numerical OEP method.[40] To test the accuracy of different local pseudopotentials, results from KSDFT-NEGF with both nonlocal and local pseudopotentials are also calculated for comparisons. Then, the ground state density distribution and effective potential are obtained by direct minimization method. Before the discussion of transport properties, we first present the ground state density distribution and potentials in real space grid.

A. Density and potential landscapes in real space

The numerical results of OFDFT simulation on one unit cell of the bcc lead are shown in Fig. 4. For comparison purpose, we have performed four different realizations of the ground state system within various schemes. There are, respectively, OFDFT with Ihm-Cohen[37] type LP (OF-LP1), OFDFT with OEP[40] type LP (OF-LP2), KSDFT with the same OEP LP (KS-LP2), and KSDFT with non-local pseudopotential (KS-NLP). In panel (a) of Fig. 4, ground state density distribution along the central z axis is plotted, where the position of one atom is shown as a black sphere for illustration.

Take the KS-NLP result as the reference, density distribution from KS-LP2 calculation has nearly the same profile (Fig. 4(a)). To be specific, the difference between them is less than 1%. Compared with the KS results, the outcomes from OFDFT are less accurate. The potential of LP2 is much harder than that of LP1 in the ion center, which leads to smaller density in the core region. OF-LP2 predicts the correct maximum position of density, but the magnitude is higher than the KS results. Difference between OF-LP2 and KS-LP2 reveals that accuracy of KEDF is the critical aspect in OFDFT, which is also the central research issue in this field. OF-LP1 only produces a smeared density distribution, which appears less preferable than the OF-LP2 result.

Apparently, it is the effective potential that determines the transport properties of a nanostructure, which is given by

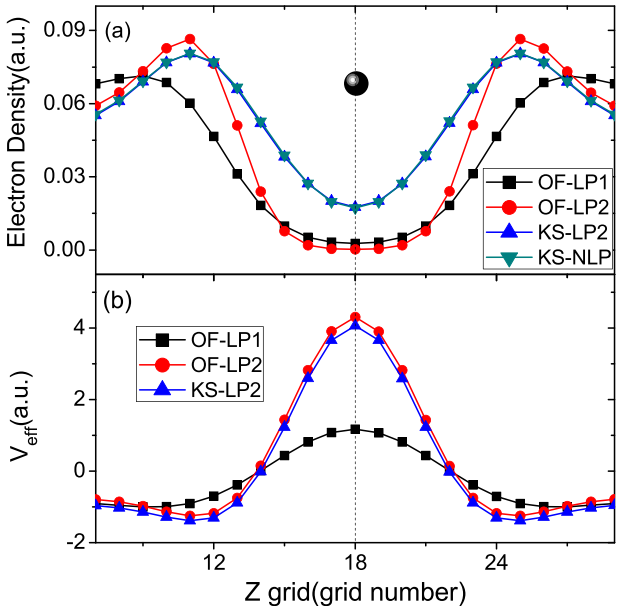

FIG. 4. Black sphere represents the silicon atom and the dashed line through the whole picture indicates its position. Panel (a) shows the density distributions along z axis, where $x = L_x/2$ and $y = L_y/2$, in four different implementations. Panel (b) plots the effective potential for calculations with local pseudopotentials. LP1 corresponds to the Ihm-Cohen type LP,[37] and LP2 is obtained from optimized effective potential method.[40]

$V_{eff} = V_{\delta H} + V_{xc} + V_{NA}$. In panel (b), we show the effective potential obtained from three different cases. The hard core of LP2 is clearly seen as high peaks in the figure. With the same local pseudopotential, OF-LP2 and KS-LP2 give very close effective potential landscapes, which is crucial in constructing the orbital space Hamiltonian defined in Eq. (21). From the results shown in panels (a) and (b), the OEP local pseudopotential is adopted in the following transport study of OFDFT method.

B. Dynamic response under finite ac bias

Compared with the dc transport, nanoscale systems show distinct properties under ac bias. For instance, a quantum electron pump generates dc current at zero bias by periodically deforming the confining potential of the system. The idea of electron pump was first proposed by Thouless[46] and then experimentally explored by Switkes and co-workers.[47] The underlying mechanism is well described by scattering matrix theory.[48] In addition, it was predicted theoretically that the charge relaxation resistance of a quantum capacitor is half of resistance quanta.[49] This was later verified experimentally in a quantum capacitor realized on 2-dimensional electron gas (2DEG), where a single spin-polarized conducting channel exists in the system.[50] Furthermore, the dynamic response of a single-walled carbon nanotube was measured at Terahertz frequencies in the experimental work, Ref. 51, and the results were well described by finite frequency ac transport theory derived within NEGF frame.[52] Recently, the dynamic admittance of a quantum dot coupled to 2DEG at different tunnel rates was measured at microwave frequencies,[53] where experimental observations are well explained by the scattering matrix theory.[54] The success of quantum transport theories in these cases consolidates the validity of these theories on predicting the ac transport properties through nanostructures.

In this section, we numerically study the dynamics response of the silicon nanostructure presented above in linear response regime.[49,55] As discussed in detail in Refs. 49, 55, and 56, the dynamic conductance can be expressed in equilibrium Green's function. Here, we investigate the frequency dependent conductance of the silicon nanostructure. It is noted that ac transport properties of a similar silicon device at low frequencies were investigated with orbital-free type method in real space using scattering matrix approach, but the leads are treated by jellium model.[17] The even-odd symmetry of dynamic conductance in Al-C_n-Al structure has been studied with the KSDFT-NEGF method.[57]

The dynamic conductance of a two-probe device under finite frequency is given by[56]

$$G_{\alpha\beta}(\omega) = G^c_{\alpha\beta}(\omega) - G^d_{\beta}(\omega)\frac{\sum_\gamma G^c_{\alpha\gamma}(\omega)}{\sum_\gamma G^d_{\gamma}(\omega)}, \tag{23}$$

where the subscripts α, β and $\gamma = L, R$ are indices of the two leads. The definition is applicable to systems near or far from equilibrium. G^c and G^d are the conductance due to the particle current and displacement current, respectively. Under the wideband condition, $G^c_{\alpha\beta}(\omega)$ is expressed in terms of the NEGF as[56]

$$G^c_{\alpha\beta}(\omega) = -\int \frac{dE}{2\pi}\frac{f-\bar{f}}{\omega}\mathrm{Tr}[-\bar{G}^r_0\Gamma_\beta G^a_0\Gamma_\alpha + \bar{G}^r_0\Gamma G^a_0\Gamma_\alpha\delta_{\alpha\beta} - i\omega\bar{G}^r_0 G^a_0\Gamma_\alpha\delta_{\alpha\beta}], \tag{24}$$

where f and $\bar{f} = f(E+\omega)$ are the Fermi distribution functions. G^r_0 and $\bar{G}^r_0$ are the retarded Green's function at energies: E and $E+\omega$. The conductance due to the displacement current is written as[56]

$$G^d_\beta(\omega) = -iq\omega\int \frac{dE}{2\pi}\frac{f-\bar{f}}{\omega}\mathrm{Tr}[\bar{G}^r_0\Gamma_\beta G^a_0]. \tag{25}$$

This term is induced by the non-equilibrium charge distribution when an ac bias is applied. One can easily verify the current conservation and gauge invariance from definition (23), which fulfills the requirements $\sum_\alpha G_{\alpha\beta} = 0$ (current conserving) and $\sum_\beta G_{\alpha\beta} = 0$ (gauge invariance).

The dynamic conductance $G_{LR}(\omega)$ of the silicon system shown in Fig. 1 is calculated based on the above definitions and the numerical results are depicted in Fig. 5. We choose subterahertz ac frequency regime $\omega \in [0, 0.25]$ THz and the system consists of two silicon atoms sandwiched between the leads. The real and imaginary parts of $G_{LR}(\omega)$ are plotted in panels (a) and (b), respectively. The results from OFDFT calculation and KSDFT simulation with both LP and NLP are also shown for comparison. In Fig. 5(a), it is observed that, real part of G_{LR} is finite at zero frequency, and increases gradually in the frequency interval. Meanwhile, imaginary part of the dynamic conductance in Fig. 5(b) starts from zero at $\omega = 0$ and grows in negative value almost linearly with the increase of frequency.

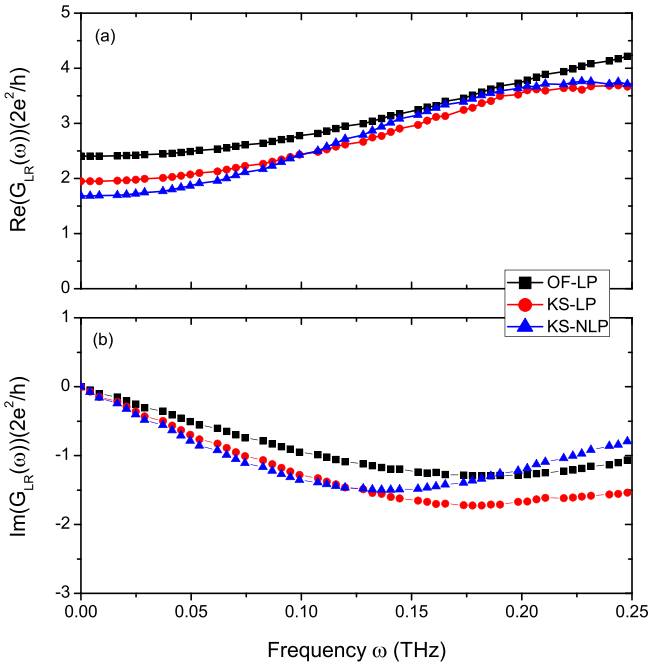

FIG. 5. Panel (a): real part of the dynamic conductance G_{LR} at different frequencies. Panel (b): imaginary part of $G_{LR}(\omega)$ versus ω. Black spheres correspond to numerical results from OFDFT calculation and red triangles are from KSDFT simulation with non-local pseudopotential. The system under investigation is the silicon nanostructure with two silicon atoms in the central region. Fermi energy is chosen to be $E_f = 0$ in the calculation.

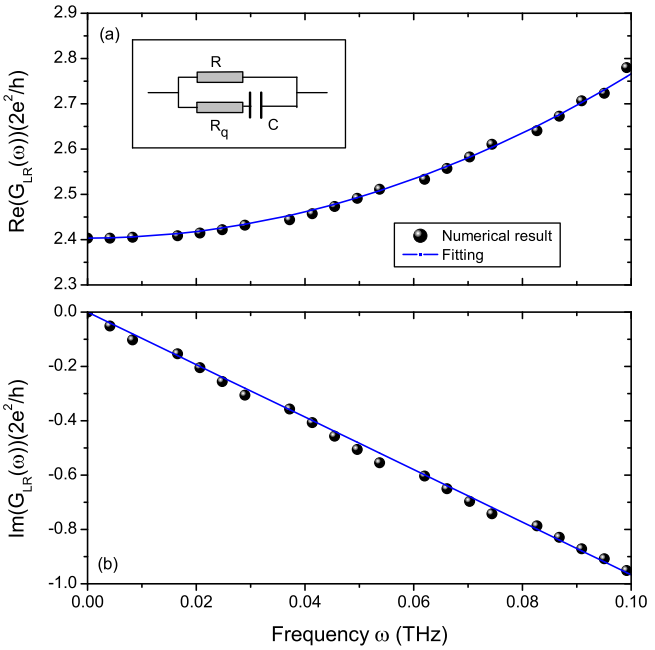

FIG. 6. Panel (a): real part of G_{LR} at different frequencies. Panel (b): imaginary part of $G_{LR}(\omega)$ versus ω. Black spheres correspond to numerical results from OFDFT calculation and the blue solid lines are fitted using Eq. (20).

Upon larger frequencies, the magnitude of $Im(G_{LR})$ starts to decrease. These general observations apply to both OF and KS results. In another word, the OF description on the silicon system is physically the same as the KS simulations. And the OF result is quantitatively comparable with the KS results with both LP and NLP. These conclusions imply that the OFDFT method is applicable in describing the equilibrium ac transport properties through the silicon nanostructure. In the following, we will focus our analysis on the physical properties of the system based on the OFDFT results.

We focus on the small frequency range $\omega \in [0, 0.1]$ THz and plot the OFDFT simulation of G_{LR} in Fig. 6. We notice that $Im(G_{LR}(\omega))$ is negative, indicating that the system shows capacitor-like behavior, although the system is transmissive with zero-frequency conductance $G_{LR}(\omega = 0) = 2.4$ in unit of $2e^2/h$.

Physically, the silicon nanostructure we studied can be modeled by the equivalent classic RC circuit shown in the inset of Fig. 6(a), whose dynamic response to ac frequency is given by

$$G(\omega) = \frac{1}{R} + \frac{1}{R_q + i/\omega C}. \tag{26}$$

Since the frequency of terahertz is a small quantity comparing with atomic energy scale, we expand the above expression in the power series of ω and obtain

$$G(\omega) = \frac{1}{R} - i\omega C + \omega^2 C^2 R_q + O(\omega^3). \tag{27}$$

Here, R stands for the dc resistance which is determined by the zero-frequency conductance, $R = 1/G_{LR}(\omega = 0)$ and R_q is the charge relaxation resistance.[49,52,58] The numerical result from OFDFT simulation is well fitted by Eq. (27), shown as the blue solid lines in Fig. 6. From Fig. 6(a), we have $R = 1/2.4\, h/2e^2$. The charge relaxation resistance R_q and capacitance C is obtained by least-square fitting of the numerical data. In the case of Fig. 6, they are $R_q = 0.39\, h/2e^2$ and $C = 4.7\, aF$, respectively. Specifically, the capacitance C is the slope of $Im(G_{LR}(\omega))$ in Fig. 6(b). These fitted parameters are valid for frequency up to 0.1 THz.

We have further investigated the dynamic response of the nanostructure with the OFDFT method when the number of silicon atoms in the silicon chain is changed. Calculation has been done for one, two, three, and four evenly spaced silicon atom(s) in the central scattering region of Fig. 1. The numerical results are included in Fig. 7. It is seen from Fig. 7(a) that the real part of dynamic conductance for different systems shares similar trend, increasing with the frequency ω, and the four curves almost parallel with each other. And with the adding of more silicon atoms, the $Re(G_{LR}(\omega))$ curves get lower and lower. In Fig. 7(b), one can see that the imaginary part of $G_{LR}(\omega)$ behaves nearly linearly as the function of the frequency. With the increasing of the silicon chain length, the magnitude of their slopes also increases. As explained above, the slope gives rise to the capacitance of the atomic system at low frequency. Clearly, all the four cases can be described by Eq. (27) with different parameters, implying that the silicon nanostructures we studied have a generic capacitive-like nature. These observations are physically interpreted as follows. Since the atomic junction is not completely transmissive, the atomic chain in the scattering region serves as a tunneling barrier and the length of the atomic chain can be viewed as the barrier width. Therefore, upon increasing the number of atoms in the atomic chain, it

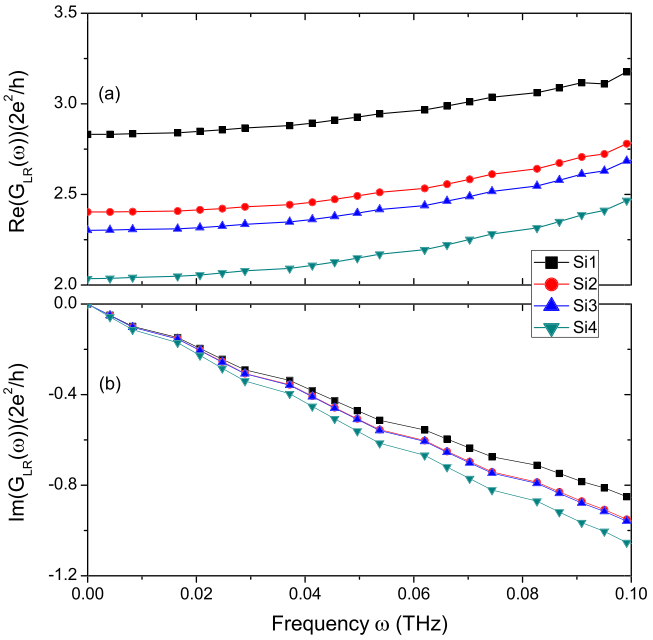

FIG. 7. Dynamic conductance $G_{LR}(\omega)$ of the silicon systems with one, two, three, and four atom(s) in the central chain. Silicon atoms in the chain are equally spaced. Fermi energy is chosen as $E_F = 0$.

gradually increases the effective barrier width thereby decreasing the dc conductance $G_{LR}(\omega = 0)$. Meanwhile, the classical capacitance of the atomic systems is slowly increased due to the charge accumulation as a result of decreasing dc conductance.

IV. CONCLUSION

In conclusion, we have used OFDFT-NEGF method to study electronic transport in nanoscale systems. Making use of the LCAO basis set, the single electron Hamiltonian is constructed from the effective potential obtained by OFDFT optimization on the scattering system. Then, the Green's function and transport properties can be calculated within the NEGF formalism. The OFDFT method is implemented on silicon nanostructures, which are atomic chains sandwiched between two monoatomic leads. The dynamic conductance of the silicon system is calculated at sub-terahertz frequency. It was found that the system responses capacitive-like to the external ac voltage. With the increasing of the number of atoms in the atomic chain, the zero-frequency conductance is suppressed and the capacitance is enhanced in the system. Our analysis shows that, up to 0.1 THz, the ac transport properties of the system are well characterized by a classic RC circuit with two resistors for dc resistance as well as charge relaxation resistance and one capacitor.

ACKNOWLEDGMENTS

We gratefully acknowledge the financial support from RGC grant (HKU 705611P), University Grant Council (Contract No. AoE/P-04/08) of the Government of HKSAR, and LuXin Energy Group. Bin Wang thanks the financial support from Shenzhen Natural Science Foundation (Grant No. JCYJ20130326111836781). Yadong Wei was supported by grant from the National Natural Science Foundation of China (Grant No. 11074171). We thank Dr. Chen Huang for useful discussion. The computational work was performed on HPCPOWER2 system of the information technology services, HKU.

[1]P. Hohenberg and W. Kohn, Phys. Rev. **136**, B864 (1964); W. Kohn and L. J. Sham, *ibid.* **140**, A1133 (1965).
[2]M. C. Payne, M. P. Teter, D. C. Allen, T. A. Arias, and J. D. Joannopoulos, Rev. Mod. Phys. **64**, 1045 (1992).
[3]G. D. Mahan, *Many Particle Physics* (Plenum Press, New York, 1990).
[4]B. G. Wang, J. Wang, and H. Guo, J. Appl. Phys. **86**, 5094 (1999); J. Taylor, H. Guo, and J. Wang, Phys. Rev. B **63**, 121104 (2001); **63**, 245407 (2001).
[5]M. Brandbyge, J.-L. Mozos, P. Ordejon, J. Taylor, and K. Stokbro, Phys. Rev. B **65**, 165401 (2002).
[6]Z. Ning and H. Guo, "MATDCAL: A first principles package for nanoelectronics modeling," in HPCS, 2008.
[7]See http://www.nanoacademic.ca/ for information about the Nanodcal software.
[8]X. Gonze, J.-M. Beuken, R. Caracas, F. Detraux, M. Fuchs, G.-M. Rignanese, L. Sindic, M. Verstraete, G. Zerah, F. Jollet, M. Torrent, A. Roy, M. Mikami, Ph. Ghosez, J.-Y. Raty, and D. C. Allan, Comput. Mater. Sci. **25**, 478–492 (2002).
[9]J. M. Soler, E. Artacho, J. D. Gale, A. García, J. Junquera, P. Ordejón, and D. Sánchez-Portal, J. Phys. Condens. Matter **14**, 2745 (2002).
[10]Y. A. Wang and E. A. Carter, in *Theoretical Methods in Condensed Phase Chemistry* (Kluwer Academic Publishers, Dordrecht, 2000), Chap. 5; G. S. Ho, V. L. Lignères, and E. A. Carter, Comput. Phys. Comm. **179**, 839 (2008).
[11]V. V. Karasiev, S. B. Trickey, and F. E. Harris, J. Comput.-Aided Mater. Des. **13**, 111 (2006); V. V. Karasiev, S. B. Trickey, and F. E. Harris, Chem. Phys. **330**, 216 (2006); S. B. Trickey, V. V. Karasiev, and R. S. Jones, Int. J. Quantum Chem. **109**, 2943 (2009); V. V. Karasiev and S. B. Trickey, Comput. Phys. Commun. **183**, 2519 (2012).
[12]L. Hung and E. A. Carter, Chem. Phys. Lett. **475**, 163 (2009).
[13]C. Huang and E. A. Carter, Phys. Rev. B **81**, 045206 (2010).
[14]C. Huang and E. A. Carter, Phys. Rev. B **85**, 045126 (2012).
[15]J. Xia, C. Huang, I. Shin, and E. A. Carter, J. Chem. Phys. **136**, 084102 (2012).
[16]J. Wang, Y. J. Wang, and H. Guo, J. Appl. Phys. **75**, 2721 (1994); Y. J. Wang, J. Wang, H. Guo, and E. Zarember, Phys. Rev. B **52**, 2738 (1995).
[17]W. Zheng, Ph.D. thesis, The University of Hong Kong, 2002.
[18]D. Vanderbilt, Phys. Rev. B **41**, 7892 (1990).
[19]J. Taylor, Ph.D thesis, McGill University, 2000.
[20]L.-W. Wang and M. P. Teter, Phys. Rev. B **45**, 13196 (1992); F. Perrot, J. Phys.: Condens. Matter **6**, 431 (1994); Y. A. Wang, N. Govind, and E. A. Carter, Phys. Rev. B **58**, 13465 (1998); Y. A. Wang, N. Govind, and E. A. Carter, *ibid.* **60**, 16350 (1999).
[21]L. H. Thomas, Proc. Cambridge Philos. Soc. **23**, 542 (1927); E. Fermi, Rend. Accad. Naz. Lincei **6**, 602 (1927); E. Fermi, Z. Phys. **48**, 73 (1928).
[22]C. F. von Weizsäcker, Z. Phys. **96**, 431 (1935).
[23]N. W. Ashcroft and N. D. Mermin, *Solid State Physics* (Thomson Learning, 1976).
[24]B. Zhou, V. L. Lignères, and E. A. Carter, J. Chem. Phys. **122**, 044103 (2005); G. S. Ho, V. L. Lignères, and E. A. Carter, Phys. Rev. B **78**, 045105 (2008).
[25]V. V. Karasiev, R. S. Jones, S. B. Trickey, and F. E. Harris, Phys. Rev. B **80**, 245120 (2009).
[26]L. Delle Site, Europhys. Lett. **86**, 40004 (2009); L. Delle Site, *ibid.* **88**, 19901(E) (2009); L. M. Ghiringhelli, I. P. Hamilton, and L. Delle Site, J. Chem. Phys. **132**, 014106 (2010); S. B. Trickey, V. V. Karasiev, and A. Vela, Phys. Rev. B **84**, 075146 (2011).
[27]J. P. Perdew, Phys. Lett. A **165**, 79 (1992).
[28]V. V. Karasiev, T. Sjostrom, and S. B. Trickey, Phys. Rev. B **86**, 115101 (2012).
[29]R. G. Parr and W. Yang, *Density-Functional Theory of Atoms and Molecules* (Oxford University Press, 1989).
[30]E. V. Ludeña and V. V. Karasiev, in *Reviews of Modern Quantum Chemistry: A Celebration of the Contributions of Robert Parr*, edited by K. D. Sen (World Scientific, Singapore, 2002).

[31]B. Fornberg, in *A Practical Guide to Pseudospectral Methods* (Cambridge University Press, 1996); J. R. Chelikowsky, N. Troullier, K. Wu, and Y. Sadd, Phys. Rev. B **50**, 11355 (1994).
[32]F. M. Xu, Ph.D. thesis, The University of Hong Kong, 2011.
[33]S. Goedecker, M. Teter, and J. Hutter, Phys. Rev. B **54**, 1703 (1996).
[34]J. P. Perdew and A. Zunger, Phys. Rev. B **23**, 5048 (1981); J. P. Perdew and Y. Wang, *ibid*. **45**, 13244 (1992); G. Ortiz and P. Ballone, Phys. Rev. Lett. **50**, 1391 (1994).
[35]J. P. Perdew, K. Burke, and M. Ernzerhof, Phys. Rev. Lett. **77**, 3865 (1996).
[36]Th. Starkloff and J. D. Joannopoulos, Phys. Rev. B **19**, 1077 (1979).
[37]J. Ihm and M. L. Cohen, Solid State Commun. **29**, 711 (1979).
[38]W. Yang and Q. Wu, Phys. Rev. Lett. **89**, 143002 (2002); Q. Wu and W. Yang, J. Chem. Phys. **118**, 2498 (2003).
[39]B. Zhou, Ph.D. thesis, University of California at Los Angeles, 2004; B. Zhou, Y. A. Wang, and E. A. Carter, Phys. Rev. B **69**, 125109 (2004).
[40]C. Huang and E. A. Carter, Phys. Chem. Chem. Phys. **10**, 7109 (2008).
[41]D. Sánchez-Portal, P. Ordejón, E. Artacho, and J. M. Soler, Int. J. Quantum Chem. **65**, 453 (1997).
[42]W. H. Press, S. A. Teukolsky, W. T. Vetterling, and B. P. Flannery, *Numerical Recipes in C: The Art of Scientific Computing* (Cambridge University Press, 1992).
[43]H. Jiang and W. Yang, J. Chem. Phys. **121**, 2030 (2004).
[44]R. H. M. Smit *et al*., Phys. Rev. Lett. **91**, 076805 (2003).
[45]S. Datta, *Electronic Transport in Mesoscopic Systems* (Cambridge University Press, 1997).
[46]D. J. Thouless, Phys. Rev. B **27**, 6083 (1983).
[47]M. Switkes *et al*., Science **283**, 1905 (1999).
[48]P. W. Brouwer, Phys. Rev. B **58**, R10135 (1998).
[49]M. Büttiker, J. Phys.: Condens. Matter **5**, 9361 (1993); M. Büttiker, A. Prêtre, and H. Thomas, Phys. Rev. Lett. **70**, 4114 (1993).
[50]J. Gabelli *et al*., Science **313**, 499 (2006).
[51]Z. Zhang *et al*., Nat. Nanotechnol. **3**, 201 (2008).
[52]D. Kienle and F. Léonard, Phys. Rev. Lett. **103**, 026601 (2009).
[53]T. Frey *et al*., Phys. Rev. B **86**, 115303 (2012).
[54]A. Prêtre, H. Thomas, and M. Büttiker, Phys. Rev. B **54**, 8130 (1996).
[55]P. W. Brouwer and M. Buttiker, Europhys. Lett. **37**, 441 (1997).
[56]B. G. Wang, J. Wang, and H. Guo, Phys. Rev. Lett. **82**, 398 (1999).
[57]B. Wang, Y. Yu, L. Zhang, Y. Wei, and J. Wang, Phys. Rev. B **79**, 155117 (2009).
[58]S. E. Nigg, R. López, and M. Büttiker, Phys. Rev. Lett. **97**, 206804 (2006); S. E. Nigg and M. Büttiker, Phys. Rev. B **77**, 085312 (2008).